Electronic Research Archive

https://www.aimspress.com/journal/era

ERA, 33(5): 2925–2946.
DOI: 10.3934/era.2025128
Received: 23 February 2025
Revised: 10 April 2025
Accepted: 15 April 2025
Published: 13 May 2025

Research article

Adaptive incremental backstepping control of stratospheric airships using time-delay estimation

Yang Sun[1], **Ming Zhu**[2], **Yifei Zhang**[2] **and Tian Chen**[2,*]

[1] School of Aeronautic Science and Engineering, Beihang University, Beijing 100191, China

[2] Institute of Unmanned System, Beihang University, Beijing 100191, China

* **Correspondence:** Email:chentian@buaa.edu.cn.

Abstract: This paper proposes an adaptive incremental backstepping control method for stratospheric airship attitude control that combines time delay estimation and incremental backstepping control to enhance robustness under model uncertainties. By integrating incremental control and time delay estimation, a linear time-invariant system relating to the attitude angle tracking error is obtained, where the time-delay estimation error is treated as a disturbance to the system. Meanwhile, an adaptive technique is utilized to reduce the effects of noise and center-of-gravity variations on system robustness. In conclusion, the convergence property of all signals is meticulously examined by employing Lyapunov theory. The proposed scheme is subsequently validated for effectiveness through numerical simulations.

Keywords: adaptive control; incremental backstepping; time-delay estimation; stratospheric airship; robust control

1. Introduction

The stratosphere, being an aerial domain yet to be fully utilized, has garnered substantial research interest [1]. Stratospheric airships, as a form of airship capitalizing on the stable atmospheric conditions within the stratosphere [1], have likewise witnessed swift advancement during this juncture [2]. Such airships are capable of executing diverse missions, including networked flight formations [3, 4] and station keeping [5]. The intrinsic dynamics of these airships are rather distinctive, exhibiting salient nonlinearities, strong coupling effects, and an inability to be accurately modeled [6]. Concurrently, the stratospheric ambience comprises numerous unpredictable perturbations. These factors render the synthesis of sophisticated control systems for the airships markedly challenging [7, 8].

Stratospheric airship control systems have reached a relatively mature stage, with commonly

adopted nonlinear control strategies including backstepping [9], sliding mode control [10], and others. These techniques are predominantly model based, relying heavily on accurate system dynamics. However, such reliance may undermine the robustness and adaptability of the control system when faced with model uncertainties or external disturbances. More adaptive and fault-tolerant control approaches may prove superior for enhancing the reliability of airship guidance systems across a wide operational envelope [11]. During the day-night cycle, airships need to adjust the ballonets and drop ballast to maintain a stable attitude, which leads to changes in the center of gravity (CG). This means existing model-based control methods have certain limitations for airship control systems. In this situation, a control method that uses acceleration to replace dynamic model parameters has been developed in aircraft control systems, called incremental nonlinear dynamic inversion (INDI) [12] and incremental backstepping (IB) [13]. A finite-time incremental backstepping method was proposed in [14], achieving rapid attitude tracking for fixed-wing aircraft while reducing dependence on model knowledge.

However, IB also has some issues that need to be addressed. First, IB requires acceleration information, while the acceleration data obtained from sensors is often noisy and needs processing before it can be applied in control systems. For this reason, the acquisition of acceleration information has always been a focus in IB research. Some have proposed a predictive filter method for this issue, but the prediction of angular acceleration requires additional modeling, and the resistance to disturbances is relatively low. Second, although IB methods have some control effects on systems with time delays, the time delay of motors is more pronounced during motor acceleration/deceleration for aircraft like airships, so the control performance of IB is average.

Time delay control (TDC) [15] implemented through time delay estimation (TDE) techniques can be viewed as a control methodology with attenuated dependence on analytical models. Similar to INDI and IB, TDC leverages time delay signals for approximating the dynamics of the governed system without explicit online identification procedures. Nevertheless, the stability guarantees for prevailing TDC architectures [16–18] impose intrinsic constraints on permissible controller gains [19], motivating conservatively narrow tuning ranges. This sufficient stability condition rigidly bounds allowable gain magnitudes from above and below. Violating said constraints risks closed-loop instability, as shown in [17, 19]. Since the constraints depend on online measurements of time-varying parameters which remain practically impossible to ascertain perfectly, conservative and suboptimal gain selections become imperative. [20] proposed a dual closed-loop control strategy combining time-delay estimation and sliding mode control to address uncertainty issues of logistics unmanned aerial vehicles (UAVs) under ground effect, crosswind disturbances, and payload variations.

Consequently, convergence rates cannot be readily improved via arbitrary tuning increments. It would thus prove significant to develop an adaptive TDC paradigm granting far less restrictive control gain faculties while preserving stability assurances. By alleviating limitations on achievable boundaries, enhanced transient performance could be attained. The synthesis of adaptive TDC schemes with expansive stable controller tuning ranges poses an open challenge to augment lag compensation capabilities for robotic and aerospace applications.

For stratospheric airships, which inherently exhibit substantial actuation latencies, effectively harnessing the time-delay dynamics to minimize actuator bandwidth requirements constitutes an important challenge in engendering high-precision, high-performance control solutions. Further research into time-delay system architectures for attenuating the control frequency demands while

preserving stability and responsiveness merits consideration across the long-endurance aerostat domain.

This paper proposes an adaptive incremental backstepping (AIBS) control scheme based on TDE for the attitude stabilization of stratospheric airships. To enhance tracking accuracy, an incremental redesign approach combining IB and adaptation is formulated. Leveraging TDE transforms the IB closed-loop dynamics into a linear architecture with the TDE discrepancy constituting a disturbance input. Concurrently, adaptation laws are synthesized to estimate the requisite angular acceleration states used by both the IB and TDE modules, with the estimations also compensating for TDE errors. Employing Lyapunov theory rigorously verifies closed-loop stability. Finally, simulations validate the efficacy of the designed methodology.

The primary contributions relative to existing literature are as follows:

1) Introduced TDE technology in stratospheric airship control systems with time-delay states by transforming TDE errors into disturbances and incorporating them into incremental controller design considerations.

2) Designed an adaptive component based on projection operators to more effectively estimate angular acceleration in cases of control matrix inaccuracies, enabling estimation and compensation of uncertain control matrix parts.

3) The control framework designed in this paper can achieve precise control of stratospheric airships under disturbance conditions, such as model uncertainty and CG offset.

The rest of this paper proceeds as follows: Section 2 delineates the dynamic modeling for stratospheric airships under nominal conditions and subject to CG deviations. Section 3 derives adaptive estimation schemes for the requisite angular acceleration states. In Section 4, the time delay matrix is formulated and stability analysis via Lyapunov theory is conducted to verify the closed-loop robustness properties of the proposed design. Section 5 presents detailed numerical simulations quantifying controller performance and comparative assessments against traditional techniques.

2. Airship dynamics modeling with CG change

During flight, an airship's CG may shift due to factors like ballast dropping. Therefore, a nonlinear model is needed to describe how changes in the CG affect the airship's characteristics.

Certain assumptions must be posited preceding the modeling of the stratospheric airship system:

Assumption 1. *Adopting the earth reference frame (ERF) as the inertial reference, the influences of spatial curvature are neglected.*

Assumption 2. *The stratospheric airship exhibits limited elastic effects [21, 22];*

Assumption 3. *Stratospheric airships constitute aerial vehicles operating in a stabilized atmospheric environment at approximate altitudes of 20 km. Buoyant lift counterbalances the gross weight to maintain airborne status [21, 22].*

The structural configuration of the stratospheric airship is depicted in Figure 1. As illustrated in the provided Figure 1, the airship is comprised of four primary components, which are: an ellipsoidal helium envelope, an empennage, propulsive propellers, and a gondola housing avionics instrumentation, as well as propulsion machinery and mission payloads. There are photovoltaic solar

arrays situated externally on the envelope to provide supplementary electrical power. Anterior positioning of four principal propulsion propellers on the aerostat enables generation of the required thrust vectoring and steering torque. In order to develop an accurate and representative airship flight dynamics model, it is imperative to rigorously define an appropriate reference coordinate system.

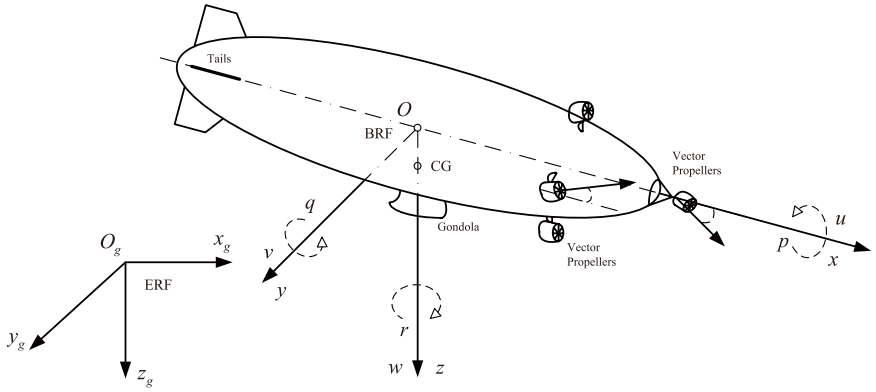

Figure 1. Stratospheric airship model.

Figure 1 delineates two specific frames of reference that are conventionally employed for analyzing the kinematics of airships: the ERF and body reference frame (BRF). The ERF constitutes a right-handed coordinate system with an origin O_g that is arbitrarily affixed at a stationary location terrestrially. The $O_g x_g$ axis of this ERF lies in the horizontal plane and is oriented facing towards north, while the $O_g z_g$ axis points vertically in the direction of the geocenter. In contrast, the BRF comprises a right-handed system with an origin O at the airship's center of buoyancy. The O_x axis of the BRF points in the forward direction through the bow, the O_z axis is directed downwards passing through the keel, and the O_y axis completes the orthogonal triad according to conventional right-hand rule conventions.

The dynamics of the airship can be reformulated as

$$\begin{cases} \dot{\boldsymbol{X}}_1 = f_1(\boldsymbol{X}_1)\boldsymbol{X}_2 \\ \dot{\boldsymbol{X}}_2 = f_2(\boldsymbol{X}_1, \boldsymbol{X}_2) + \boldsymbol{B}\boldsymbol{\tau} \end{cases} \tag{2.1}$$

where $\boldsymbol{X}_1 = [x, y, -z, \phi, \theta, \psi]^{\mathrm{T}}$, $\boldsymbol{X}_2 = [u, v, w, p, q, r]^{\mathrm{T}}$, $\boldsymbol{\tau} = \left[\tau_u, \tau_v, \tau_w, \tau_p, \tau_q, \tau_r\right]^{\mathrm{T}}$ represents the vector of all state quantities in the airship control system. Details of the control function can be seen in Eqs (2.2)–(2.4)

$$f_1(\boldsymbol{X}_1) = \begin{bmatrix} \boldsymbol{K} & \boldsymbol{0}_{3\times 3} \\ \boldsymbol{0}_{3\times 3} & \boldsymbol{R} \end{bmatrix} \tag{2.2}$$

$$\boldsymbol{f}_2(\boldsymbol{X}_1, \boldsymbol{X}_2) = [\boldsymbol{F}_v, \boldsymbol{F}_w]^{\mathrm{T}} + [\boldsymbol{f}_v, \boldsymbol{f}_\omega]^{\mathrm{T}} \tag{2.3}$$

$$\boldsymbol{B} = \begin{bmatrix} \boldsymbol{B}_{11} & \boldsymbol{B}_{12} \\ \boldsymbol{B}_{21} & \boldsymbol{B}_{22} \end{bmatrix} \tag{2.4}$$

where

$$\boldsymbol{K} = \begin{bmatrix} \mathrm{c}\theta\mathrm{c}\psi & \mathrm{s}\theta\mathrm{c}\psi\,\mathrm{s}\phi - \mathrm{s}\psi\mathrm{c}\phi & \mathrm{s}\theta\mathrm{c}\psi\mathrm{c}\phi + \mathrm{s}\psi\,\mathrm{s}\phi \\ \mathrm{c}\theta\,\mathrm{s}\psi & \mathrm{s}\theta\,\mathrm{s}\psi\,\mathrm{s}\phi + \mathrm{c}\psi\mathrm{c}\phi & \mathrm{s}\theta\,\mathrm{s}\psi\mathrm{c}\phi - \mathrm{c}\psi\,\mathrm{s}\phi \\ -\mathrm{s}\theta & \mathrm{c}\theta\,\mathrm{s}\phi & \mathrm{c}\theta\mathrm{c}\phi \end{bmatrix} \tag{2.5}$$

is the direction cosine matrix for transformation from BRF to ERF and $s()$ and $c()$ represent sin and cos, respectively.

$$\boldsymbol{R} = \begin{bmatrix} 1 & \sin\phi\tan\theta & \cos\phi\tan\theta \\ 0 & \cos\phi & -\sin\phi \\ 0 & \sin\phi\sec\theta & \cos\phi\sec\theta \end{bmatrix} \tag{2.6}$$

is the Euler rotation matrix. The specific modeling, parameters, and details of the remaining control effectiveness matrix are comprehensively presented in reference [23] Appendix B.

Therefore, the attitude dynamics equation of the airship can be obtained as follows:

$$\begin{cases} \dot{\boldsymbol{\Theta}} = \boldsymbol{K}\boldsymbol{\Omega} & \text{(2.7a)} \\ \dot{\boldsymbol{\Omega}} = \boldsymbol{F}_\omega + \boldsymbol{B}_{22}\boldsymbol{\tau}_\omega + \boldsymbol{B}_{21}\boldsymbol{\tau}_u + \boldsymbol{f}_\omega + \boldsymbol{\delta}_\omega & \text{(2.7b)} \end{cases}$$

where $\boldsymbol{\Theta} = [\phi, \theta, \psi]^{\mathrm{T}}$, $\boldsymbol{\Omega} = [p, q, r]^{\mathrm{T}}$.

The diurnal temperature fluctuations intrinsically induce variations in the CG location of stratospheric airships due to structural effects. Under the condition of the CG offset of Δz_C, the functions $\mathcal{F}_w$ and $\mathcal{B}_{22}$ admit decomposition into known and unknown parts, expressible as $\mathcal{F}_w = \boldsymbol{F}_w + \Delta\boldsymbol{F}_w$ and $\mathcal{B}_{22} = \boldsymbol{B}_{22} + \Delta\boldsymbol{B}_{22}$. The terms $\boldsymbol{F}_w \in \mathbb{R}^{n\times 1}$ and $\boldsymbol{B}_{22} \in \mathbb{R}^{n\times n}$ constitute the known dynamic functions employed in synthesizing the control law. The quantities $\Delta\boldsymbol{F}_w$ and $\Delta\boldsymbol{B}_{22}$ represent model uncertainties, implying the exact functional forms are inaccessible. In other words, when accounting for modeling uncertainties, the control matrix of the dynamical model should be expressed in the following form:

$$\begin{cases} \boldsymbol{F}_w = \mathcal{F}_w - \Delta\boldsymbol{F}_w \\ \boldsymbol{B}_{22} = \mathcal{B}_{22} - \Delta\boldsymbol{B}_{22} \end{cases} \tag{2.8}$$

Assumption 4. *In practical scenarios, upper bounds exist on $\Delta\boldsymbol{F}_w$ and $\Delta\boldsymbol{B}_{22}$. Specifically, $|\Delta\boldsymbol{F}_w|_\infty \leq \bar{F}_w$ and $|\Delta\boldsymbol{B}_{22}|\infty \leq \bar{B}_{22}$,where $\bar{F}_w$ and $\bar{B}_{22}$ denote the supremum norms of $\Delta\boldsymbol{F}_w$ and $\Delta\boldsymbol{B}_{22}$, respectively.*

Assumption 5. *([24]) There exists $c_M \in \mathbb{R} > 0$, such that the reference signal $\boldsymbol{X}$ satisfies $\left\|\dot{\boldsymbol{X}}\right\| \leq c_M$, where $\|\cdot\|$ denotes 2-norm of a vector or a matrix.*

Remark 1. *Assuming the smoothness of reference signals is a plausible conjecture commonly employed in relevant studies, as non-smooth reference signals can induce abrupt changes in actuators, potentially leading to damage in mechanical systems.*

3. Adaptive angular velocity estimator

Given the prohibitive procurement costs and constrained accessibility of angular accelerometers, angular acceleration measurements are routinely approximated via numerical differentiation of preprocessed angular velocity data. Due to the inherent limitations in instrumentation and signal processing, the measured angular accelerations $\dot{\boldsymbol{\Omega}}$ invariably comprise metrological distortions $\dot{\boldsymbol{\Omega}}_\delta$, stochastic noise components $\dot{\boldsymbol{\Omega}}_\sigma$, and deviations induced by temporal lags $\dot{\boldsymbol{\Omega}}_r$.

To streamline controller synthesis, the airship dynamics are rendered in the following affine form:

$$\begin{cases} \dot{\boldsymbol{\Theta}} = \boldsymbol{K}\boldsymbol{\Omega} & \text{(3.1a)} \\ \dot{\boldsymbol{\Omega}} = \boldsymbol{F}_\omega + \boldsymbol{B}_{22}\boldsymbol{\tau}_\omega + \boldsymbol{\delta}_\omega & \text{(3.1b)} \end{cases}$$

where $\boldsymbol{\delta}_\omega = \boldsymbol{B}_{21}\boldsymbol{\tau}_u + \dot{\boldsymbol{\Omega}}_\delta + \dot{\boldsymbol{\Omega}}_\sigma + \dot{\boldsymbol{\Omega}}_r$ represent the coupled terms and superimposed noise terms of different types in the dynamical modeling of airships.

A preliminary estimation of the angular accelerations is formulated as follows:

$$\hat{\dot{\boldsymbol{\Omega}}}_0 = \boldsymbol{F}_{w_0} + \boldsymbol{B}_{22}\boldsymbol{\tau}_{w_0} + \boldsymbol{B}_{21}\boldsymbol{\tau}_{u_0} \tag{3.2}$$

Equation (3.2) furnishes accurate estimates of the angular accelerations under idealized conditions where $\Delta\boldsymbol{F}_{w_0} = 0$ and $\Delta\boldsymbol{B}_{22} = 0$ hold regardless of the noise. However, in practical flight scenarios, intrinsic disturbances unavoidably introduce uncertainties into the vehicle model, exemplified by CG variations. Since such model uncertainties are excluded in the formulation of Eq (3.2) , the resulting estimated accelerations $\hat{\dot{\boldsymbol{\Omega}}}_0$ lose fidelity.

The Figure 2 illustrates the AIBS control framework, which consists of an outer loop and an inner loop. The outer loop includes four key components: angular acceleration estimation, angular velocity controller, attitude dynamics, and attitude kinematics. These modules work together to regulate the system's angular motion and ensure stable attitude control. The inner loop focuses on handling Disturbance, which represents external or internal perturbations affecting the system's performance.

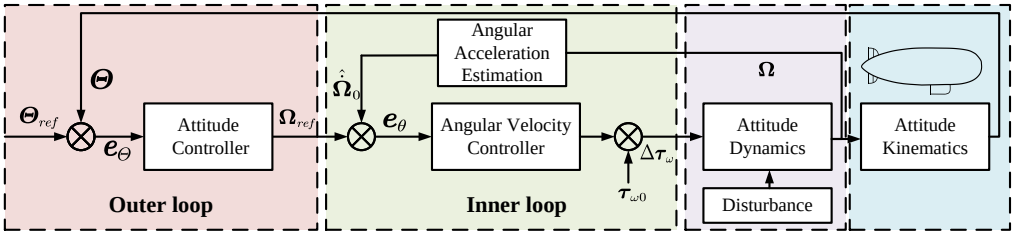

Figure 2. Block diagram of the AIBS control framework.

This Figure 3 outlines the structure of an adaptive angular velocity estimator, which dynamically adjusts its parameters to improve tracking performance. The system incorporates an adaptation mechanism that continuously refines key estimates, such as disturbance terms and control gains, based on real-time error feedback.

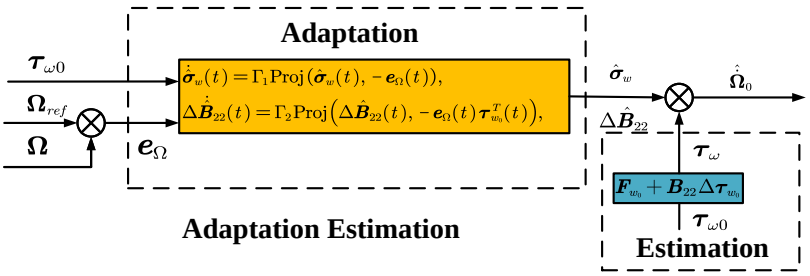

Figure 3. Block diagram of adaptive angular velocity estimator.

To rectify this deficiency, a compensatory element is synthesized to account for angular acceleration errors stemming from CG shifts and unmodeled dynamics. From an estimation perspective, the true disturbed angular rate kinetics are representable as follows:

$$\dot{\boldsymbol{\Omega}} = \boldsymbol{F}_w + \Delta\boldsymbol{F}_w + \boldsymbol{B}_{22}\boldsymbol{\tau}_w + \Delta\boldsymbol{B}_{22}\boldsymbol{\tau}_w + \boldsymbol{\delta}_w \tag{3.3}$$

Inspection of the angular accelerations described in Eq (3.3) indicates the presence of metrological distortions, thereby demonstrating the inadequacy of the angular rate kinetics. These distortions significantly degrade the performance and instability in the angular rate controller implemented. To mitigate this deficiency, a salient approach involves formulating an estimator for the angular accelerations by harnessing existing informative data.

Therefore, the expression for the current angular acceleration is obtained as follows:

$$\dot{\boldsymbol{\Omega}}_0 = \boldsymbol{F}_{w_0} + \Delta\boldsymbol{F}_{w_0} + \boldsymbol{B}_{22}\Delta\boldsymbol{\tau}_{w_0} + \Delta\boldsymbol{B}_{22}\boldsymbol{\tau}_{w_0} + \boldsymbol{\delta}_{w_0} \tag{3.4}$$

where $\Delta\boldsymbol{F}_{w_0} \in \mathbb{R}^{3\times1}$ and $\Delta\boldsymbol{B}_{22}(\omega) \in \mathbb{R}^{3\times3}$ constitute the model uncertainties, $\boldsymbol{\tau}_{w_0} \in \mathbb{R}^{3\times1}$ to serve as the input to the current attitude control channel. The quantity $\boldsymbol{\delta}_{w_0} \in \mathbb{R}^{3\times1}$, as characterized by Eq (3.4) , signifies the unknown disturbance. Owing to the independence from control input, $\boldsymbol{\delta}_{w_0}$ and $\Delta\boldsymbol{F}_{w_0}$ are denoted by the aggregate term $\boldsymbol{\sigma}_{w_0}(\omega)$ for conciseness, yielding:

$$\dot{\boldsymbol{\Omega}}_0 = \boldsymbol{F}_{w_0} + \boldsymbol{B}_{22}\Delta\boldsymbol{\tau}_{w_0} + \Delta\boldsymbol{B}_{22}\boldsymbol{\tau}_{w_0} + \boldsymbol{\sigma}_{w_0} \tag{3.5}$$

Assume the angular rate magnitudes are bounded as $\|\boldsymbol{\Omega}(t)\| \le \bar{\Omega}$, where $\bar{\Omega}$ is a known upper limit. Under this boundedness condition, the model uncertainties are posited to comply with Assumptions 6 and 7.

Assumption 6. *The model uncertainties are bounded as follows:*

$$\boldsymbol{\sigma}_w \in \Theta_\sigma, \Delta\boldsymbol{B}_{22} \in \Theta_{\boldsymbol{B}}, \|\boldsymbol{\sigma}_w\| \le \lambda_\sigma, \|\Delta\boldsymbol{B}_{22}\| \le \lambda_{\boldsymbol{B}} \tag{3.6}$$

where Θ_σ and $\Theta_{\boldsymbol{B}}$ denote known convex compact sets representing uncertainty domains, and λ_σ, $\lambda_{\boldsymbol{B}}$ are known upper bounds on $|\boldsymbol{\sigma}_w|$ and $|\Delta\boldsymbol{B}_{22}|$, respectively.

Assumption 7. *We consider the boundedness of the derivatives of the model uncertainties. Specifically, we have the following:*

$$\left\|\frac{\partial\boldsymbol{\sigma}_w}{\partial\omega}\right\| \le d_\sigma < \infty, \qquad \left\|\frac{\partial\Delta\boldsymbol{B}_{22}}{\partial\omega}\right\| \le d_{\boldsymbol{B}} < \infty \tag{3.7}$$

where d_σ and $d_{\boldsymbol{B}}$ denote known upper bounds on the derivatives of the model uncertainties $\sigma_d(\omega)$ and $\Delta\boldsymbol{B}_{22}$, respectively.

Furthermore, to facilitate the design of the adaptive law, we invoke the projection operator as delineated in [25] and formalized in Definition 1.

Definition 1. *Let us consider a convex compact set defined as follows:*

$$\Omega_C = [\theta_1, \theta_2, \ldots, \theta_n]^{\mathrm{T}}, \quad \theta_i \in [\theta_i^{\min}, \theta_i^{\max}], \quad i = 1, 2, \ldots, n \tag{3.8}$$

where $\theta_i^{\max}$ and $\theta_i^{\min}$ represent the upper and lower bounds. We define ε as a sufficiently small positive constant that satisfies $\theta_i^{\min} + \varepsilon \le \theta_i \le \theta_i^{\max} - \varepsilon$.

Now, let us introduce the projection operator, denoted as $\mathrm{Proj}(*,*)$*, defined as follows:*

$$\mathrm{Proj}(\alpha_i, \beta_i) = \begin{cases} \frac{\alpha_i^{\max} - \alpha_i}{\varepsilon}\|\beta_i\|, & \text{if } \alpha_i > \alpha_i^{max} - \varepsilon \\ \frac{\alpha_i - \alpha_i^{\min}}{\varepsilon}\|\beta_i\|, & \text{if } \alpha_i < \alpha_i^{\min} + \varepsilon \\ \beta_i, & \text{else} \end{cases} \tag{3.9}$$

As per Definition 1, the following equation is valid:

$$(\theta - \theta^*)\,(\mathrm{Proj}(\theta, y) - y) \le 0, \quad y, \theta^* \in \mathbb{R}^n \tag{3.10}$$

Under CG shifts and external disturbances, the estimated angular accelerations in Eq (3.10) are corrected as follows:

$$\hat{\dot{\boldsymbol{\Omega}}}_0 = \boldsymbol{F}_{w_0} + \boldsymbol{B}_{22}\Delta\boldsymbol{\tau}_{w_0} + \Delta\hat{\boldsymbol{B}}_{22}\boldsymbol{\tau}_{w_0} + \hat{\boldsymbol{\sigma}}_{w_0} \tag{3.11}$$

where $\hat{\dot{\boldsymbol{\Omega}}}_0$ denotes the estimated angular accelerations at time t_0, $\hat{\boldsymbol{\sigma}}_{w_0} \in \mathbb{R}^{3\times1}$ and $\Delta\hat{\boldsymbol{B}}_{22} \in \mathbb{R}^{3\times3}$ represent the estimated uncertainty terms $\boldsymbol{\sigma}_{w_0}$ and $\Delta\boldsymbol{B}_{22}$ obtained from the adaptive law in Eq (3.12).

Considering $\boldsymbol{\Omega}_d$ as the desired reference for the inner attitude control loop, $\boldsymbol{e}_\Omega = \boldsymbol{\Omega}_d - \boldsymbol{\Omega}$ representing the error signal to the attitude control system, an adaptive angular acceleration estimation method is designed as follows:

$$\begin{aligned} &\dot{\hat{\boldsymbol{\sigma}}}_w(t) = \Gamma_1\,\mathrm{Proj}\left(\hat{\boldsymbol{\sigma}}_w(t), -\boldsymbol{e}_\Omega(t)\right), && \hat{\boldsymbol{\sigma}}_w(0) = [0,0,0]^{\mathrm{T}} \\ &\Delta\dot{\hat{\boldsymbol{B}}}_{22}(t) = \Gamma_2\,\mathrm{Proj}\left(\Delta\hat{\boldsymbol{B}}_{22}(t), -\boldsymbol{e}_\Omega(t)\boldsymbol{\tau}_{w_0}^{\mathrm{T}}(t)\right), && \Delta\hat{\boldsymbol{B}}_{22}(0) = 0 * \text{ eye (3)} \end{aligned} \tag{3.12}$$

where Γ_1 and Γ_2 are positive adaptation gains, which are directly proportional to the convergence rate of the error.

4. Incremental backstepping control with TDE design

The primary focus of this subsection is the temporal actuation latency arising within the electric motor apparatus. To counteract the pernicious impacts of this motor delay on system performance, an incremental backstepping controller architecture based on TDE techniques is proposed herein, constituting the pivotal contribution of this work.

Step 1: Let $\boldsymbol{\Theta}_d$ represent the input desired attitude reference, $\boldsymbol{e}_\theta = \boldsymbol{\Theta} - \boldsymbol{\Theta}_d$ denote the tracking error for the signal $\boldsymbol{\Theta}$. For (3.1a), we construct the virtual control signal $\boldsymbol{\Omega}_d$ as follows:

$$\boldsymbol{\Omega}_d = -\boldsymbol{K}^{-1}(\boldsymbol{K}_1\boldsymbol{e}_\theta - \dot{\boldsymbol{\Theta}}_d) \tag{4.1}$$

where $\boldsymbol{K}_1 \in \mathbb{R} > 0$ represents a design parameter.

Denoting $\boldsymbol{e}_\Omega = \boldsymbol{\Omega} - \boldsymbol{\Omega}_d$ as the tracking error for (3.1b), the dynamics of the tracking error $\boldsymbol{e}_\theta$ becomes the following:

$$\begin{aligned} \dot{\boldsymbol{e}}_\theta &= \dot{\boldsymbol{\Theta}} - \dot{\boldsymbol{\Theta}}_d = \boldsymbol{K}\boldsymbol{\Omega} - \dot{\boldsymbol{\Theta}}_d \\ &= \boldsymbol{K}(\boldsymbol{\Omega}_d + \boldsymbol{e}_\Omega) - \dot{\boldsymbol{\Theta}}_d \end{aligned} \tag{4.2}$$

Step 2: Consider the second subsystem (3.3), since the effects of center of mass shifts and noise on the dynamics have been addressed as $\Delta\boldsymbol{B}_{22}$ in Eq (3.11), the following considers the impacts introduced by model uncertainties in $\boldsymbol{B}_{22}$.

To mitigate reliance on the analytical model, including terms $\boldsymbol{F}_\omega$ and $\boldsymbol{B}_{22}$, this study implements TDE methods. Moreover, formulating the Step 2 controller under backstepping procedures necessitates a strict-feedback architecture.

By introducing a constant diagonal matrix $\bar{\boldsymbol{B}}_{22}$, an alternative expression of $\boldsymbol{B}_{22}$ is obtained as follows:

$$\bar{\boldsymbol{B}}_{22}^{-1}\dot{\boldsymbol{\Omega}} = \boldsymbol{H}(\boldsymbol{\Omega}, \dot{\boldsymbol{\Omega}}, \boldsymbol{\Theta}, \dot{\boldsymbol{\Theta}}) + \boldsymbol{\tau}_{\omega}. \tag{4.3}$$

where $\boldsymbol{H}(\boldsymbol{\Omega}, \dot{\boldsymbol{\Omega}}, \boldsymbol{\Theta}, \dot{\boldsymbol{\Theta}}) = \left(\bar{\boldsymbol{B}}_{22}^{-1} - \boldsymbol{B}_{22}^{-1}\right)\dot{\boldsymbol{\Omega}} + \boldsymbol{B}_{22}^{-1}\boldsymbol{F}_{\omega}$ can be estimated by the TDE as

$$\hat{\boldsymbol{H}}(\boldsymbol{\Omega}, \dot{\boldsymbol{\Omega}}, \boldsymbol{\Theta}, \dot{\boldsymbol{\Theta}}) = \boldsymbol{H}(\boldsymbol{\Omega}_0, \dot{\boldsymbol{\Omega}}_0, \boldsymbol{\Theta}_0, \dot{\boldsymbol{\Theta}}_0) = \bar{\boldsymbol{B}}_{22}^{-1}\dot{\boldsymbol{\Omega}}_0 - \boldsymbol{\tau}_{\omega 0}, \tag{4.4}$$

where $\boldsymbol{\Omega}_0$, $\dot{\boldsymbol{\Omega}}_0$, $\boldsymbol{\Theta}_0$, $\dot{\boldsymbol{\Theta}}_0$, and $\boldsymbol{\tau}_{\omega_0}$ denote the states $\boldsymbol{\Omega}$, $\dot{\boldsymbol{\Omega}}$, $\boldsymbol{\Theta}$, $\dot{\boldsymbol{\Theta}}$, and control $\boldsymbol{\tau}_{\omega}$ at the prior sampling instance, respectively. As substantiated in [26], under adequately high sampling rates surpassing 30 times the system bandwidth, a discretized controller exhibits analogous dynamics to the continuous-time counterpart. Hence, given sufficiently fast sampling, the nonlinearity can be approximated via TDE techniques.

From (4.3) and (4.4), we derive the following strict-feedback system with the incremental controller $\Delta\boldsymbol{\tau}_{\omega}$:

$$\dot{\boldsymbol{\Omega}} = \dot{\boldsymbol{\Omega}}_0 + \left(\bar{\boldsymbol{B}}_{22} + \Delta\boldsymbol{B}_{22}\right)\Delta\boldsymbol{\tau}_{\omega} + \boldsymbol{\epsilon} \tag{4.5}$$

where $\Delta\boldsymbol{\tau}_{\omega} = \boldsymbol{\tau}_{\omega} - \boldsymbol{\tau}_{\omega 0}, \boldsymbol{\epsilon} = \bar{\boldsymbol{B}}_{22}(\boldsymbol{H}(\boldsymbol{\Omega}, \dot{\boldsymbol{\Omega}}, \boldsymbol{\Theta}, \dot{\boldsymbol{\Theta}}) - \hat{\boldsymbol{H}}(\boldsymbol{\Omega}, \dot{\boldsymbol{\Omega}}, \boldsymbol{\Theta}, \dot{\boldsymbol{\Theta}}))$ is the TDE error. For the strict-feedback system (4.5) and (3.11), $\Delta\boldsymbol{\tau}_{\omega}$ is designed as

$$\Delta\boldsymbol{\tau}_{\omega} = \bar{\boldsymbol{B}}_{22}^{-1}\left(-\boldsymbol{K}_2\boldsymbol{e}_{\Omega} - \boldsymbol{K}\boldsymbol{e}_{\theta} + \dot{\boldsymbol{\Omega}}_d - \hat{\dot{\boldsymbol{\Omega}}}_0 - \boldsymbol{\epsilon}\right) \tag{4.6}$$

where $\boldsymbol{K}_2 \in \mathbb{R} > 0$ is a design parameter. Substituting (4.6) into (4.5) yields

$$\begin{aligned}
\boldsymbol{e}_{\Omega} &= \dot{\boldsymbol{\Omega}}_d - \dot{\boldsymbol{\Omega}} \\
&= \dot{\boldsymbol{\Omega}}_d - \left(\boldsymbol{\Omega}_0 + \boldsymbol{\mathcal{B}}_{22}\bar{\boldsymbol{B}}_{22}^{-1}\left(\boldsymbol{K}_2\boldsymbol{e}_{\Omega} - \boldsymbol{K}\boldsymbol{e}_{\theta} - \boldsymbol{\epsilon} + \dot{\boldsymbol{\Omega}}_d - \hat{\dot{\boldsymbol{\Omega}}}_0\right)\right) \\
&= \dot{\boldsymbol{\Omega}}_d - \left(\dot{\boldsymbol{\Omega}}_0 + \left(\bar{\boldsymbol{B}}_{22} + \Delta\boldsymbol{B}_{22}\right)\bar{\boldsymbol{B}}_{22}^{-1}\left(\boldsymbol{K}_2\boldsymbol{e}_{\Omega} - \boldsymbol{K}\boldsymbol{e}_{\theta} - \boldsymbol{\epsilon} + \dot{\boldsymbol{\Omega}}_d - \hat{\dot{\boldsymbol{\Omega}}}_0\right)\right) \\
&= -\boldsymbol{K}_2\boldsymbol{e}_{\Omega} + \boldsymbol{K}\boldsymbol{e}_{\theta} + \tilde{\boldsymbol{\sigma}}_w + \Delta\tilde{\boldsymbol{B}}_{22}\boldsymbol{\tau}_{\omega} - \boldsymbol{\xi}
\end{aligned} \tag{4.7}$$

where $\boldsymbol{\xi} = \boldsymbol{\epsilon} - \Delta\boldsymbol{B}_{22}\Delta\tau_w$. Given a sufficiently high sampling frequency, $\boldsymbol{\xi}$ can be neglected as inconsequential.

Thus, the tracking error dynamics $\boldsymbol{e}_{\Omega}$ are rendered stable given practical bounds on the TDE discrepancy term $\boldsymbol{\epsilon}$, as formally established in the subsequent lemma. Analogous to analyses in [26], the impending result characterizes the boundedness properties of the TDE error within a sufficiently fast sampled implementation:

Lemma 1. *Given an adequately high sampling rate, there exists a positive constant* $\bar{\epsilon} \in \mathbb{R} > 0$ *such that* $\|\boldsymbol{\epsilon}\| \leq \bar{\epsilon}$ *is satisfied, provided that* $\bar{\boldsymbol{B}}_{22}$ *fulfills* $\left\|\boldsymbol{I} - \bar{\boldsymbol{B}}_{22}\bar{\boldsymbol{B}}_{22}^{-1}\right\| < 1$. *This boundedness of the TDE error* ϵ *follows from the selection of a constant* $\bar{\boldsymbol{B}}_{22}$ *that approximates the nonlinear function* $\boldsymbol{B}_{22}$ *with sufficiently small error, along with the use of the AIBS controller design that stabilizes the system dynamics.*

Consequently, the updated control law for angular rate AIBS, as defined in Eq (4.6), can be expressed as follows:

$$\boldsymbol{\tau}_{\omega} = \boldsymbol{\tau}_{\omega 0} + \Delta\boldsymbol{\tau}_{\omega} \tag{4.8}$$

Given the bounded TDE discrepancy, closed-loop stability is analyzed via the Lyapunov function $\boldsymbol{V}_1 = \frac{1}{2}\boldsymbol{e}_\theta^{\mathrm{T}}\boldsymbol{e}_\theta + \frac{1}{2}\boldsymbol{e}_\Omega^{\mathrm{T}}\boldsymbol{e}_\Omega$. Invoking the tracking error dynamics in (4.2) and (4.6), the Lyapunov derivative $\dot{\boldsymbol{V}}_1$ is expressed as follows:

$$\begin{aligned}\dot{\boldsymbol{V}}_1 =& \frac{1}{2}\boldsymbol{e}_\theta^{\mathrm{T}}\boldsymbol{e}_\theta + \frac{1}{2}\boldsymbol{e}_\Omega^{\mathrm{T}}\boldsymbol{e}_\Omega + \tilde{\boldsymbol{\sigma}}_w^{\mathrm{T}}\tilde{\boldsymbol{\sigma}}_w + \mathrm{trace}\left(\Delta\tilde{\boldsymbol{B}}_{22}^{\mathrm{T}}\Delta\tilde{\boldsymbol{B}}_{22}\right)\\ =& -\boldsymbol{K}_1\boldsymbol{e}_\theta^{\mathrm{T}}\boldsymbol{e}_\theta + \boldsymbol{e}_\theta^{\mathrm{T}}\boldsymbol{K}\boldsymbol{e}_\Omega + \boldsymbol{e}_\Omega^{\mathrm{T}}\dot{\boldsymbol{e}}_\Omega + \boldsymbol{e}_\Omega^{\mathrm{T}}\tilde{\boldsymbol{\sigma}}_w + \boldsymbol{e}_\Omega^{\mathrm{T}}\Delta\tilde{\boldsymbol{B}}_{22}u_0\\ &+ \tilde{\boldsymbol{\sigma}}_w^{\mathrm{T}}\dot{\tilde{\boldsymbol{\sigma}}}_w + \mathrm{trace}\left(\Delta\tilde{\boldsymbol{B}}_{22}^{\mathrm{T}}\Delta\dot{\tilde{\boldsymbol{B}}}_{22}\right)\\ =& -\boldsymbol{K}_1\boldsymbol{e}_\theta^{\mathrm{T}}\boldsymbol{e}_\theta - \boldsymbol{K}_2\boldsymbol{e}_\Omega^{\mathrm{T}}\boldsymbol{e}_\Omega + \boldsymbol{e}_\Omega^{\mathrm{T}}\boldsymbol{\epsilon} + \tilde{\boldsymbol{\sigma}}_w^{\mathrm{T}}\left(\boldsymbol{e}_\Omega^{\mathrm{T}} + \dot{\hat{\boldsymbol{\sigma}}}_w\right)\\ &+ \Delta\hat{\boldsymbol{B}}_{22}^{\mathrm{T}}\left(\boldsymbol{e}_\Omega^{\mathrm{T}}u_0 + \Delta\dot{\hat{\boldsymbol{B}}}_{22}\right) - \tilde{\boldsymbol{\sigma}}_w^{\mathrm{T}}\dot{\boldsymbol{\sigma}}_w - \Delta\hat{\boldsymbol{B}}_{22}^{\mathrm{T}}\Delta\dot{\boldsymbol{B}}_{22} - \boldsymbol{e}_\Omega^{\mathrm{T}}\boldsymbol{\xi}\end{aligned} \tag{4.9}$$

Through Young's inequality [24] and Lemma 1, we have

$$\boldsymbol{e}_\Omega^{\mathrm{T}}\boldsymbol{\xi} \le 0.5\boldsymbol{e}_\Omega^{\mathrm{T}}\boldsymbol{e}_\Omega + 0.5\boldsymbol{\xi}^{\mathrm{T}}\boldsymbol{\xi} \le 0.5\boldsymbol{e}_\Omega^{\mathrm{T}}\boldsymbol{e}_\Omega + 0.5\bar{\xi}^2 \tag{4.10}$$

The utilization of the projection operator guarantees that $\tilde{\boldsymbol{\sigma}}_w$ is confined within the constraint set Θ_σ, and $\Delta\tilde{\boldsymbol{B}}_{22}$ is restricted to the constraint set $\Theta_{\boldsymbol{B}}$, for all instances when $t \ge 0$. Significantly, this ensures that the tracking errors remain bounded in a uniform manner.

$$\|\boldsymbol{K}_1\boldsymbol{e}_\theta^{\mathrm{T}}\boldsymbol{e}_\theta + (\boldsymbol{K}_2 - 0.5)\boldsymbol{e}_\Omega^{\mathrm{T}}\boldsymbol{e}_\Omega + 0.5\bar{\epsilon}^2\| \le \sqrt{\frac{\chi_1}{\Gamma_1} + \frac{\chi_2}{\Gamma_2}}, \quad \forall t > 0 \tag{4.11}$$

with

$$\begin{aligned}\chi_1 &\triangleq 2\lambda_\sigma^2 + \lambda_\sigma d_\sigma,\\ \chi_2 &\triangleq 2\max_{\Delta\boldsymbol{B}\in\Theta_{\boldsymbol{B}}}\mathrm{trace}\left(\Delta\boldsymbol{B}_{22}^{\mathrm{T}}(\omega)\Delta\boldsymbol{B}_{22}(\omega)\right) + \max\|\Delta\boldsymbol{B}_{22}(\omega)\|d_{\boldsymbol{B}}\end{aligned} \tag{4.12}$$

Lemma 2. *The Lyapunov function is expressed as follows:*

$$\boldsymbol{V}_1 \le \frac{\chi_1}{\Gamma_1} + \frac{\chi_2}{\Gamma_2} \tag{4.13}$$

Proof. At the initial moment, it can be demonstrated that

$$\boldsymbol{V}_1(0) \le \frac{1}{\Gamma_1}\lambda_\sigma^2 + \frac{1}{\Gamma_2}\max_{\Delta\boldsymbol{B}\in\Theta_{\boldsymbol{B}}}\mathrm{trace}\left(\Delta\boldsymbol{B}_{22}^{\mathrm{T}}(\omega)\Delta\boldsymbol{B}_{22}(\omega)\right) < \frac{\chi_1}{\Gamma_1} + \frac{\chi_2}{\Gamma_2} \tag{4.14}$$

The projection operators, as described in Eq (3.9), guarantee the boundedness of the estimations of model uncertainties $\hat{\boldsymbol{\sigma}}_w(t)$ and $\Delta\hat{\boldsymbol{B}}_{22}(t)$ for all $t \ge 0$. The specific details are provided below:

$$\begin{aligned}&\max\left(\frac{1}{\Gamma_1}\tilde{\boldsymbol{\sigma}}_w^{\mathrm{T}}(t)\tilde{\boldsymbol{\sigma}}_w(t) + \frac{1}{\Gamma_2}\mathrm{trace}\left(\Delta\tilde{\boldsymbol{B}}_{22}^{\mathrm{T}}(t)\Delta\tilde{\boldsymbol{B}}_{22}(t)\right)\right)\\ &\le \frac{1}{\Gamma_1}\lambda_\sigma^2 + \frac{1}{\Gamma_2}\max_{\Delta\boldsymbol{B}\in\Theta_{\boldsymbol{B}}}\mathrm{trace}\left(\Delta\boldsymbol{B}_{22}^{\mathrm{T}}(\omega)\Delta\boldsymbol{B}_{22}(\omega)\right)\end{aligned} \tag{4.15}$$

$$\begin{aligned}&-\frac{1}{\Gamma_1}\tilde{\boldsymbol{\sigma}}_w^{\mathrm{T}}(t)\dot{\boldsymbol{\sigma}}_w(t) - \frac{1}{\Gamma_2}\mathrm{trace}\left(\Delta\tilde{\boldsymbol{B}}_{22}^{\mathrm{T}}(t)\Delta\dot{\boldsymbol{B}}_{22}(t)\right)\\ &\le \frac{1}{\Gamma_1}\lambda_\sigma d_\sigma + \frac{1}{\Gamma_2}\max\|\Delta\boldsymbol{B}_{22}(\omega)\|d_{\boldsymbol{B}}\end{aligned} \tag{4.16}$$

Suppose that at any given time t_1, the condition $\boldsymbol{V}_1(t_1) > \chi_1/\Gamma_1 + \chi_2/\Gamma_2$ holds. By combining Eqs (4.10) and (4.12), we obtain the following:

$$\boldsymbol{K}_1\boldsymbol{e}_\theta^{\mathrm{T}}\boldsymbol{e}_\theta + (\boldsymbol{K}_2 - 0.5)\boldsymbol{e}_\Omega^{\mathrm{T}}\boldsymbol{e}_\Omega + 0.5\bar{\epsilon}^2 > \frac{2}{\Gamma_1}\lambda_\sigma d_\sigma + \frac{2}{\Gamma_2}\max\|\Delta\boldsymbol{B}_{22}(\omega)\|d_{\boldsymbol{B}} \tag{4.17}$$

Thus, $\dot{\boldsymbol{V}}_1(t_1) < 0$. In conclusion, for all $t \geq 0$, the Lyapunov function satisfies $\boldsymbol{V}_1(t) \leq \chi_1/\Gamma_1 + \chi_2/\Gamma_2$. This completes the proof. □

Significantly, the projection operator plays a crucial role in the adaptive law by mitigating angular acceleration errors and ensuring their stability within a specified range.The utilization of AIBS methodology integrates angular acceleration estimation with IB, eliminating the necessity for numerical differentiation in the estimation procedure. Consequently, this integration effectively mitigates potential complications arising from time delays and amplification of sensor noise.

The utilization of the adaptive law in the AIBS framework allows for relaxation in the requirement of precise aerodynamic parameter knowledge. Instead, deviations in these parameters can be corrected by the adaptive law itself. As a result, the AIBS method reduces the dependency on accurate model information. Furthermore, disturbances and time delays caused by instrumentation can be compensated within predefined limits through the adaptive law. In comparison to the conventional IB approach, AIBS demonstrates superior tracking performance.

5. Simulation results and analysis

The objective of this section is to assess the effectiveness and resilience of the proposed AIBS controller design in the face of diverse interference mechanisms, such as mismatched disturbances, degraded sensor sampling rates, and parametric uncertainty. To effectively validate the proposed method's effectiveness and ensure comparability across all simulation experiments, identical initial conditions were established. Specifically, the initial state was uniformly set to $\boldsymbol{\Theta} = [5, 5, 10]^{\mathrm{T}}$. The total simulation experiment duration was set to 1000 s, with the final expected values for the first 500 s set to $\boldsymbol{\Theta}_d = [0, 0, 45]^{\mathrm{T}}$. Subsequently, during the remaining 500 s, the final expected values were adjusted to $\boldsymbol{\Theta}_d = [0, 5, 60]^{\mathrm{T}}$. In addition, comparative evaluations are performed against baseline IB from [13] and time-delay estimation from [27] combined with incremental backstepping method (TIBS) . The legend labeled "cmd" in the result figures represents the ariation curve of expected attitude angles. The control parameters for the competing designs are delineated in Table 1. These contrast studies demonstrate the superiority of the AIBS controller in furnishing enhanced tracking accuracy and robustness across the range of destabilizing effects examined.

Table 1. Airship model related data and controller parameters selection.

ρ_{ref}	0.088 kg/m^3	m_{ref}	9400 kg
l_{ref}	38 m	g	9.74 m/s^2
C_d	0.5	S_{ref}	1134 m^2
$[I_x, I_y, I_z]$	$[2, 5.5, 5.5] \times 10^6$	$\boldsymbol{K}_1$	0.005
$[x_C, y_C, z_C]$	[0, 0, 0.5] m	$\boldsymbol{K}_2$	100
$[G, B]$	[91556, 91556] N	Γ_1	5
$[c_p, c_q, c_r]$	$[1, 10, 17] \times 10^{-3}$	Γ_2	10

5.1. *Influence of model uncertainties*

For stratospheric airships, due to the currently unclear stratospheric environment and complex situations such as fluid-solid coupling, there are often uncertainties in aerodynamic parameters. To evaluate the effectiveness of the designed method under model uncertainty, a 20% error was introduced into the aerodynamic parameters. In other words, in this simulation section, the stratospheric airship aerodynamic model used is 80% of the conventional model. Figures 4–6 show the angle, angular velocity, and control channel responses under IB, TIBS, and AIBS control methods. Table 2 displays the convergence times for these methods under aerodynamic parameter uncertainty.

From Table 2, it is evident that AIBS has faster convergence compared to the other two methods, demonstrating excellent tracking performance. The AIBS control method enhanced its robustness to model inaccuracies through its inherent adaptivity and reduced dependence on precise system parameter knowledge. Therefore, under conditions of model uncertainties, the AIBS structure exhibits higher control precision compared to the standard IB control method.

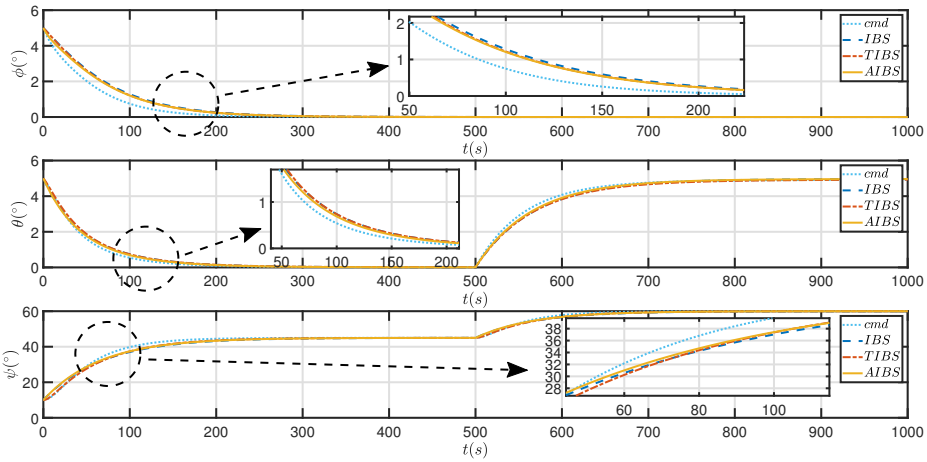

Figure 4. Angular response dynamics under conditions of model uncertainties.

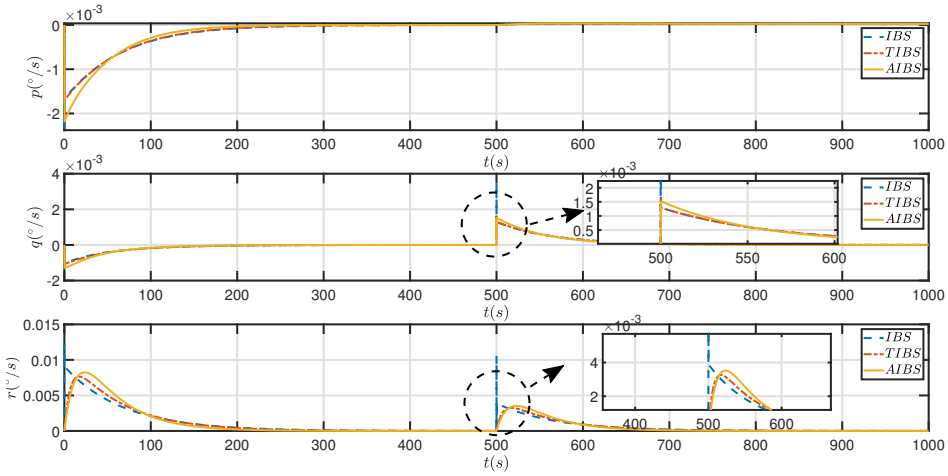

Figure 5. Angular rate response dynamics under conditions of model uncertainties.

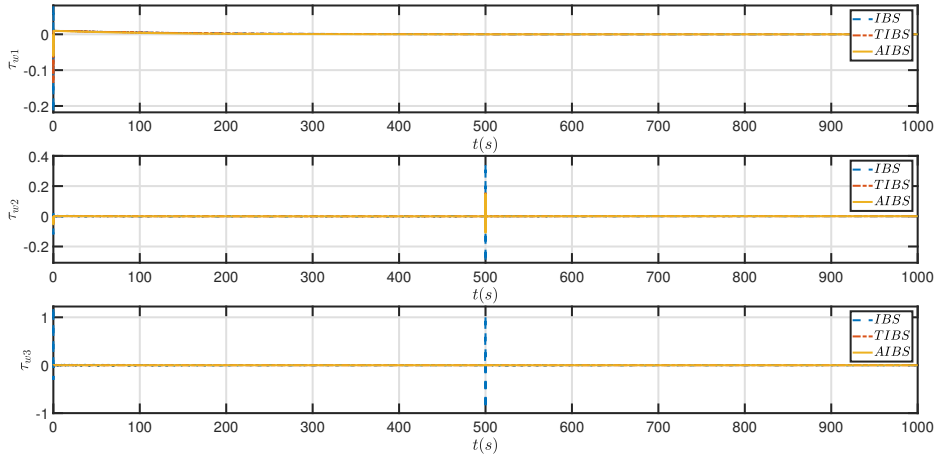

Figure 6. Control channel response dynamics under conditions of model uncertainties.

Table 2. Influence of model uncertainties convergence time (s).

	ϕ	θ(first)	ψ(first)	θ(second)	ψ(second)
AIBS	297.6	304.8	3172	902.8	779.2
TIBS	315.7	328.4	386.6	955.5	810.5
IB	346.1	357.8	379.6	967.0	817.3

5.2. Time delay disturbance

Due to signal transmission processes, data delays may occur. This research assumes a 10-millisecond motor response delay affecting angular rate feedback signals during telemetry. Under these delay conditions, the performance of the AIBS controller is compared with traditional IB and TIBS compensators. The resulting angle, angular acceleration, and control channel response dynamics are shown in Figures 7–9. Table 3 displays the convergence times for these methods under time delay.

As shown in Figure 7, the uncompensated IB controller exhibits a longer response delay in the controlled system, primarily due to reduced real-time performance caused by measurement delays in angular rate and acceleration feedback signals. In contrast, under TIBS and AIBS control methods, angular rate dynamics remain stable. The TIBS controller reduces the impact of measurement delay by synchronizing angular acceleration signals, though its dynamic response sensitivity is somewhat reduced. The AIBS controller compensates for delay-induced errors through an adaptive mechanism, enabling faster tracking of angular rate trajectories compared to the TIBS method, thus demonstrating stronger sensor delay robustness. Since the IB control method does not handle time delay, the time delay has the most significant impact on the IB method. From the convergence conditions of θ and ψ in Table 3, it can be observed that the IB method does not achieve convergence before switching the expected values.

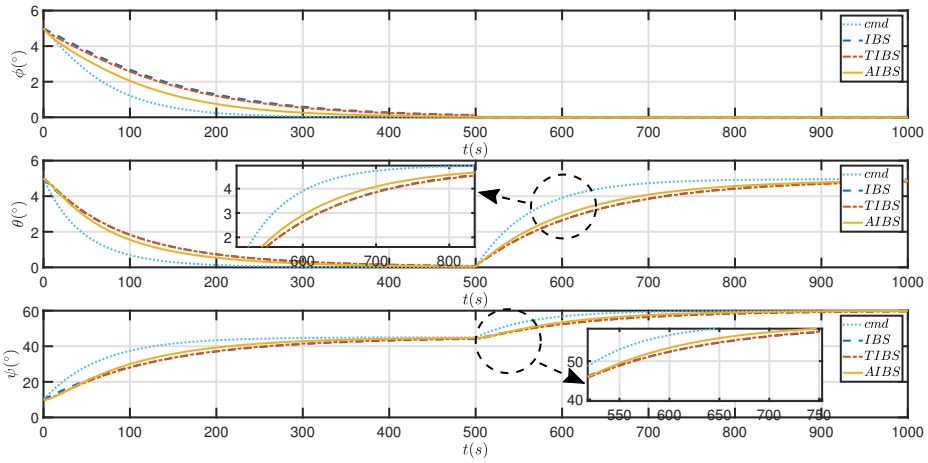

Figure 7. Angular response dynamics under conditions of time delay.

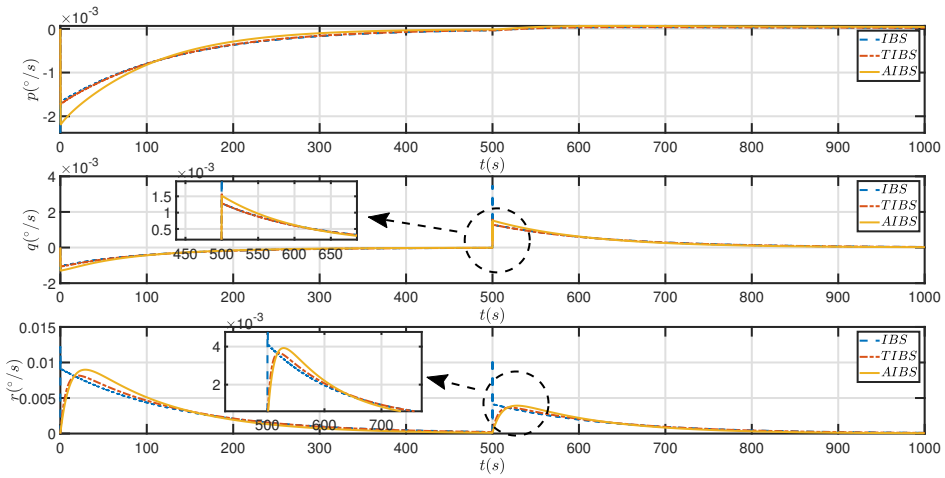

Figure 8. Angular rate response dynamics under conditions of time delay.

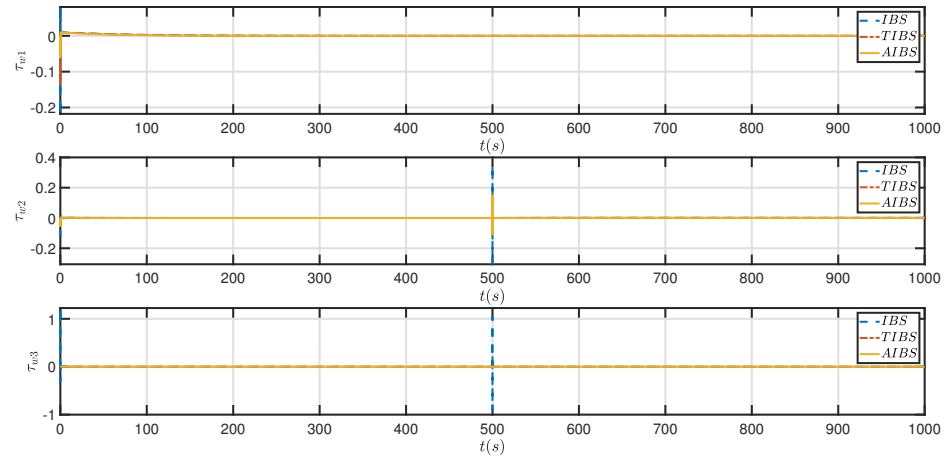

Figure 9. Control channel response dynamics under conditions of time delay.

Table 3. Time delay disturbance convergence time (s).

	ϕ	θ(first)	ψ(first)	θ(second)	ψ(second)
AIBS	488.5	426.4	447.7	956.2	803.2
TIBS	502.8	489.0	495.4	979.9	854.4
IB	513.6	Not converged	Not converged	Not converged	Not converged

5.3. Influence of CG changes

This section primarily investigates the effectiveness of the proposed control method under CG movement conditions. Specifically, sudden CG shifts can lead to significant performance degradation and induce angular rate oscillations, particularly in pitch and roll channels. More severe CG movements can trigger more pronounced angular rate fluctuations. The CG movement scenarios are shown in Table 4. The angle, angular acceleration, and control channel responses under AIBS control with CG offset are depicted in Figures 10–18.

Table 4. CG shift specification dataset.

	Δx	Δy	Δz
$Case1$	0.5 m	0.1 m	0.1 m
$Case2$	0.1 m	0.5 m	0.1 m
$Case3$	0.1 m	0.1 m	0.5 m

From Tables 5–7, it can be observed that under the AIBS compensator, attitude angles can rapidly converge to the equilibrium state even during CG movement and the system maintains excellent dynamic tracking performance, further verifying the inherent robustness of the AIBS method to such disturbances.

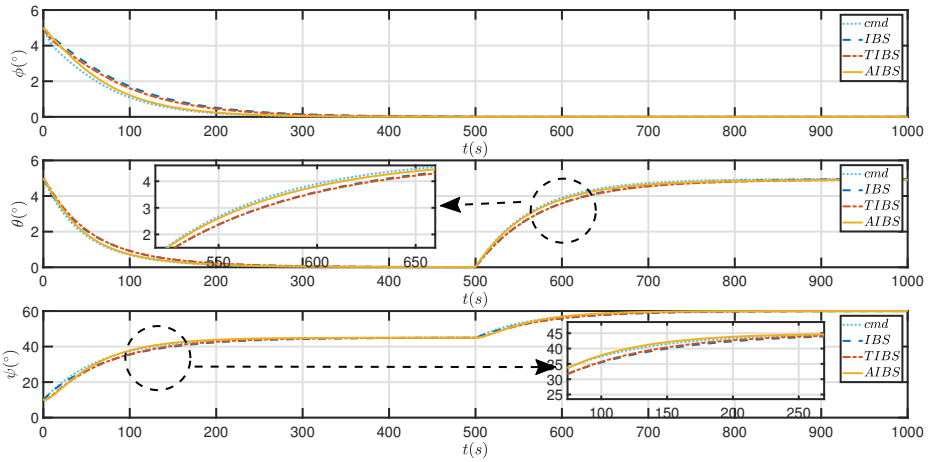

Figure 10. Angular response dynamics under condition $Case1$.

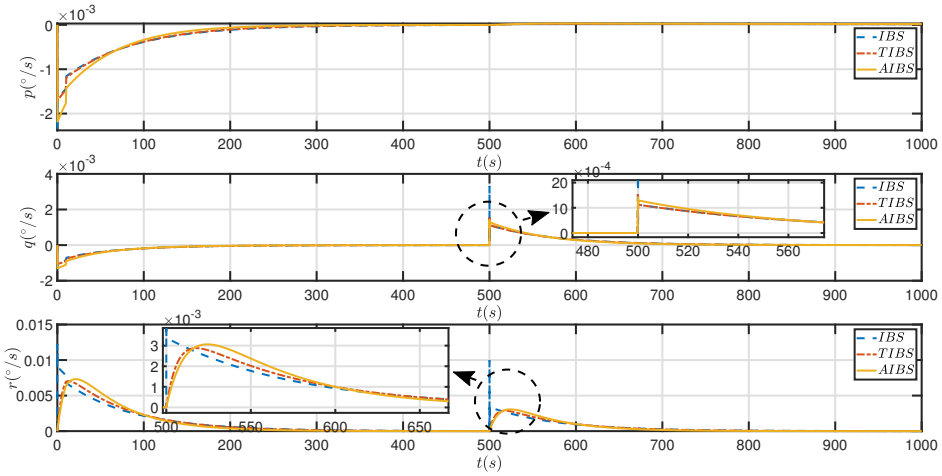

Figure 11. Angular rate response dynamics under condition *Case*1.

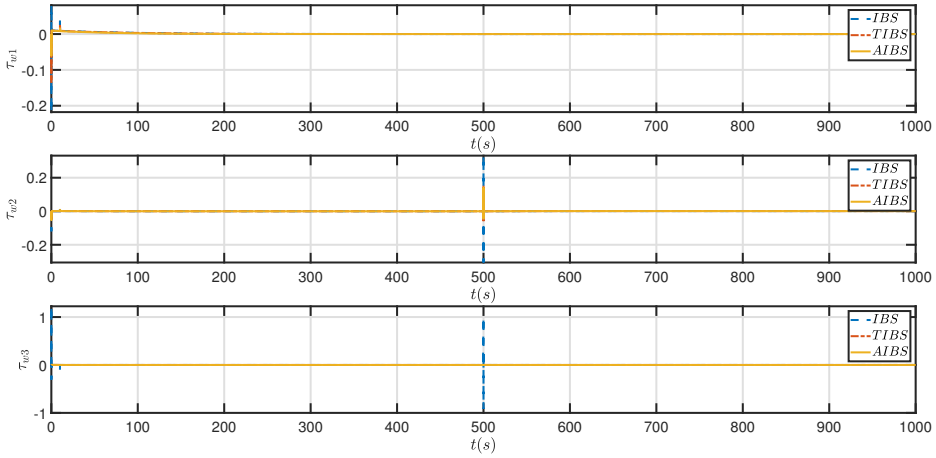

Figure 12. Control channel response dynamics under condition *Case*1.

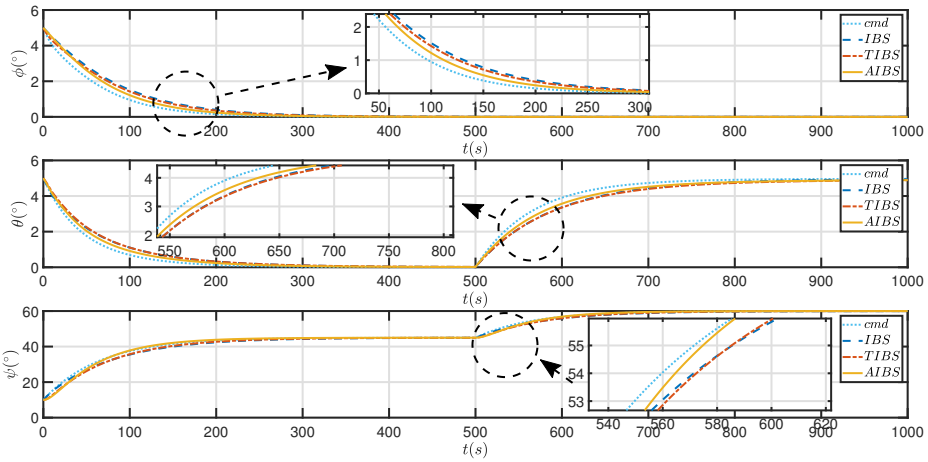

Figure 13. Angular rate response dynamics under condition *Case*2.

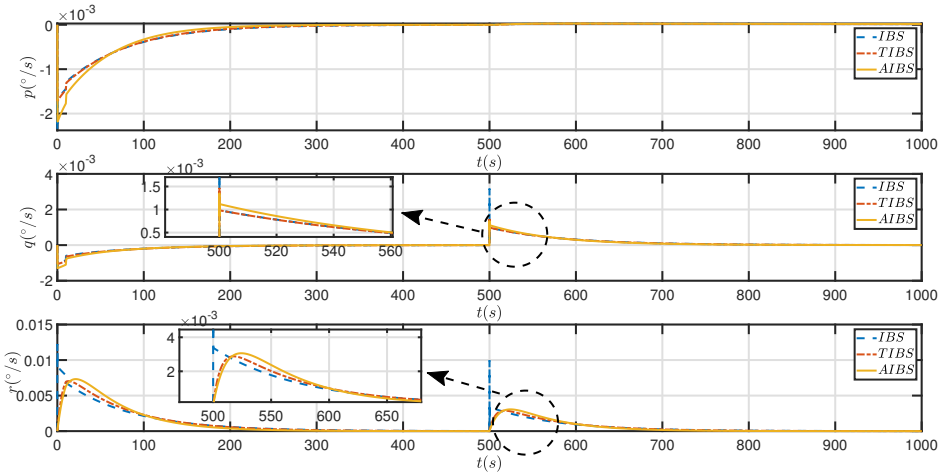

Figure 14. Angular response dynamics under condition *Case*2.

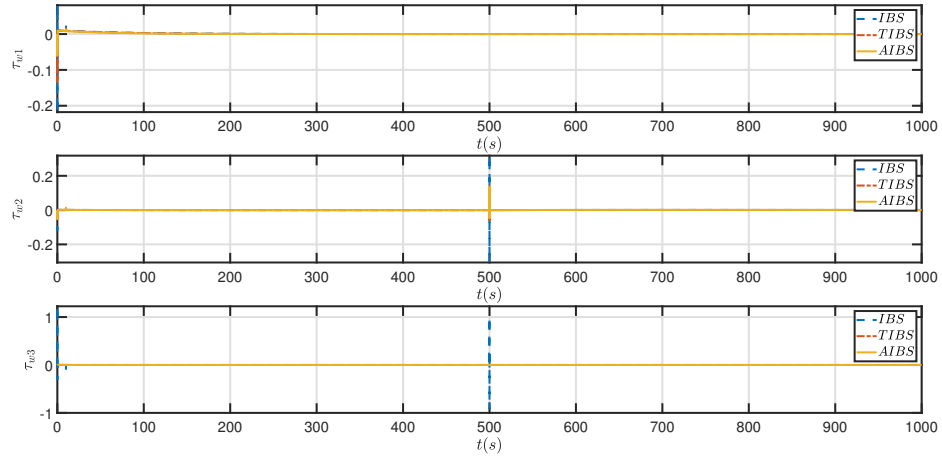

Figure 15. Control channel response dynamics under condition *Case*2.

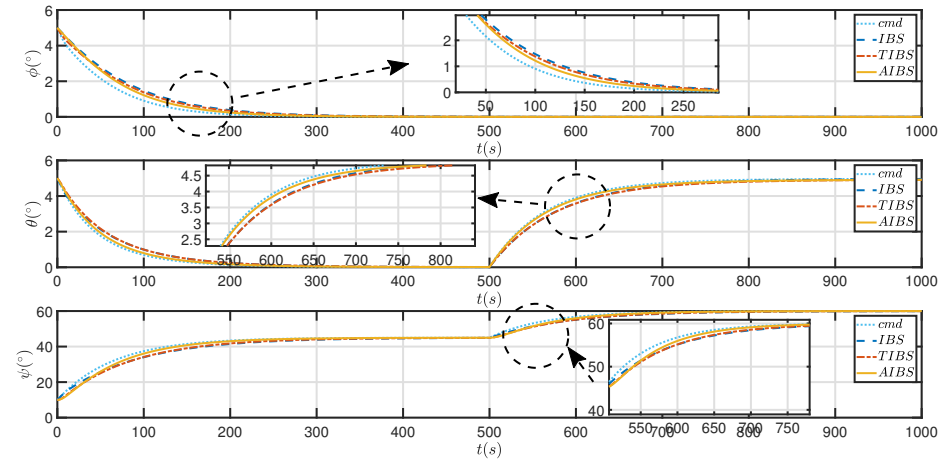

Figure 16. Angular response dynamics under condition *Case*3.

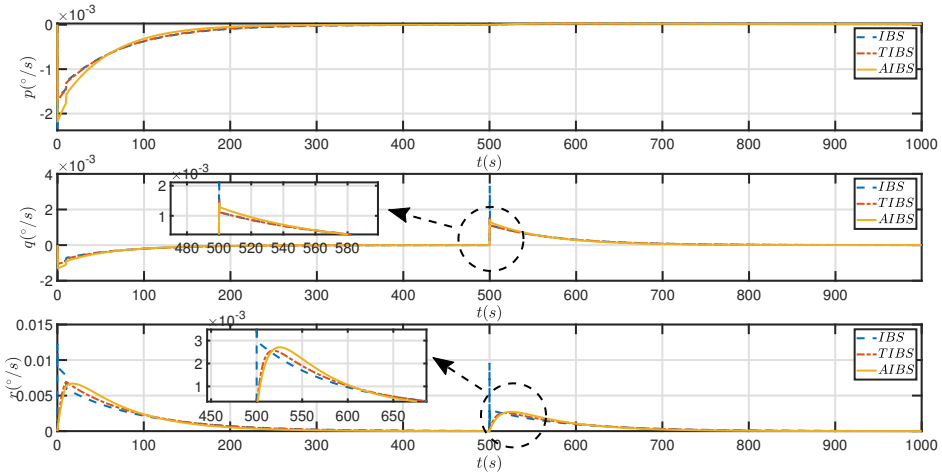

Figure 17. Angular rate response dynamics under condition *Case*3.

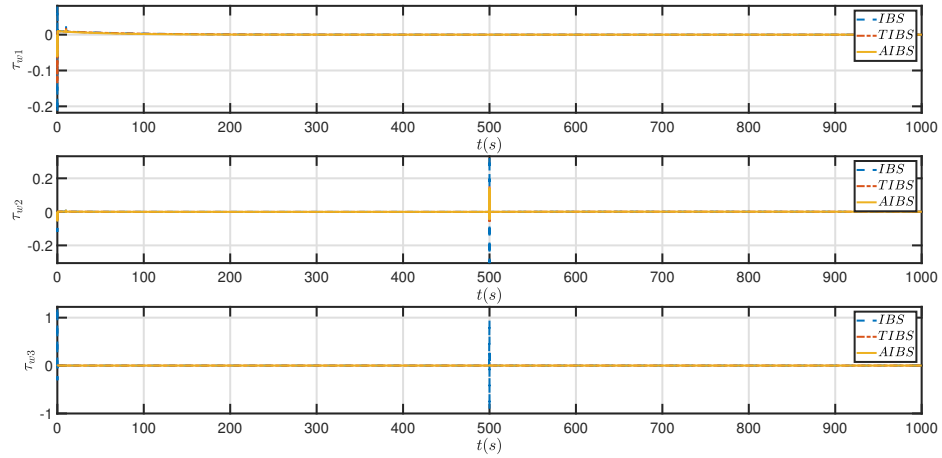

Figure 18. Control channel response dynamics under condition *Case*3.

These results validate the AIBS technology's strong robustness to CG shifts and its ability to suppress related tracking degradation. Additionally, Figures 13–18 provide a further comparative assessment of the AIBS control method against traditional IB and TIBS controls under CG Cases 2 and 3.

Table 5. Condition *Case*1 convergence time (s).

	ϕ	θ(first)	ψ(first)	θ(second)	ψ(second)
AIBS	478.0	312.6	405.6	932.1	793.1
TIBS	509.2	324.8	432.7	971.8	824.8
IB	519.4	360.8	484.5	989.2	833.9

Table 6. Condition $Case2$ convergence time (s).

	ϕ	θ(first)	ψ(first)	θ(second)	ψ(second)
AIBS	328.5	424.7	385.1	923.9	794.5
TIBS	355.4	435.8	392.4	956.3	827.2
IB	404.3	457.9	415.2	978.9	849.6

Table 7. Condition $Case3$ convergence time (s).

	ϕ	θ(first)	ψ(first)	θ(second)	ψ(second)
AIBS	388.5	350.1	420.3	935.7	823.8
TIBS	402.9	367.8	447.2	964.0	839.4
IB	423.8	379.4	457.3	988.2	876.1

By comparing Cases 1–3, it can be concluded that CG movements along the x-axis, y-axis, and z-axis have the most significant impacts on ϕ, θ, and ψ, respectively. In particular, when moving along the x-axis, the convergence time of attitude angles increases dramatically, with convergence times being 1.45 and 1.23 times those of Cases 2 and 3, respectively.

6. Conclusions

This research has presented an AIBS for stratospheric airship control methodology exhibiting resilience against multiple destabilizing effects prevalent in real-world implementations. Specifically, the proposed technique demonstrates an innate capacity to attenuate the performance degradation stemming from sensor delays, telemetry noise, as well as model parameter uncertainties. This is achieved via online estimation and compensation of the coupled error dynamics within an incremental nonlinear control architecture.

The results have verified the ability of AIBS control to significantly outperform conventional nonlinear dynamic inversion designs under nonoptimal conditions like external disturbances or CG shifts. Moreover, in the presence of input lags and output signal distortions, the developed angular rate controller succeeded in achieving rapid setpoint tracking without sustained oscillations. The augmented time-delay estimation and command conditioning modules have proven essential to guaranteeing tracking accuracy and stability margins under broad operating scenarios.

Additionally, the model-free adaptive estimation feature inherent to AIBS control reduces reliance on high-fidelity analytical models, simplifying compensator synthesis protocols, and bolstering resilience against unmodeled effects. This research provides promising evidence that AIBS and related delay-centric paradigms could play an integral role in next-generation aerospace and robotic control systems necessitating stability and peak performance in the face of adverse environments.

Future research should focus on extending the validation of AIBS methodologies, including guidance law and fault-tolerant control system development under expanded anomalous conditions. The practical implementation and flight-testing of AIBS architectures also constitutes an open problem requiring cross-disciplinary efforts in years ahead.

Use of AI tools declaration

The authors declare they have not used Artificial Intelligence (AI) tools in the creation of this article.

Acknowledgments

This work was supported by the National Natural Science Foundation of China (Grant No. 52402509).

Conflict of interest

The authors declare there is no conflicts of interest.

References

1. X. Yang, X. Yang, X. Deng, Horizontal trajectory control of stratospheric airships in wind field using Q-learning algorithm, *Aerosp. Sci. Technol.*, **106** (2020), 106100. https://doi.org/10.1016/j.ast.2020.106100
2. M. Manikandan, R. S. Pant, A comparative study of conventional and tri-lobed stratospheric airships, *Aeronaut. J.*, **125** (2021), 1434–1466. https://doi.org/10.1017/aer.2021.24
3. J. H. Kim, S. J. Yoo, Distributed event-triggered adaptive formation tracking of networked uncertain stratospheric airships using neural networks, *IEEE Access*, **8** (2020), 49977–49988. https://doi.org/10.1109/ACCESS.2020.2979995
4. E. Price, M. J. Black, A. Ahmad, Viewpoint-driven formation control of airships for cooperative target tracking, *IEEE Rob. Autom. Lett.*, **8** (2023), 3653–3660. https://doi.org/10.1109/LRA.2023.3264727
5. L. Chen, Q. Gao, Y. Deng, J. Liu, Moving-mass-based station keeping of stratospheric airships, *Aeronaut. J.*, **125** (2021), 1231–1244. https://doi.org/10.1017/aer.2021.9
6. Z. Zheng, Z. Guan, Y. Ma, B. Zhu, Constrained path-following control for an airship with uncertainties, *Eng. Appl. Artif. Intell.*, **85** (2019), 295–306. https://doi.org/10.1016/j.engappai.2019.06.021
7. Y. Yang, A time-specified nonsingular terminal sliding mode control approach for trajectory tracking of robotic airships, *Nonlinear Dyn.*, **92** (2018), 1359–1367. https://doi.org/10.1007/s11071-018-4131-3
8. Y. Wu, Q. Wang, D. Duan, W. Xie, Y. Wei, Neuroadaptive output-feedback trajectory tracking control for a stratospheric airship with prescribed performance, *Aeronaut. J.*, **124** (2020), 1568–1591. https://doi.org/10.1017/aer.2020.54
9. J. Yuan, M. Zhu, X. Guo, W. Lou, Finite-time trajectory tracking control for a stratospheric airship with full-state constraint and disturbances, *J. Franklin Inst.*, **358** (2021), 1499–1528. https://doi.org/10.1016/j.jfranklin.2020.12.010

10. A. Saeed, Y. Liu, M. Z. Shah, L. Wang, Z. Zuo, Q. Wang, Higher order sliding mode based lateral guidance and control of finless airship, *Aerosp. Sci. Technol.*, **113** (2021), 106670. https://doi.org/10.1016/j.ast.2021.106670
11. D. Cui, C. K. Ahn, Y. Sun, Z. Xiang, Mode-dependent state observer-based prescribed performance control of switched systems, *IEEE Trans. Circuits Syst. II: Express Briefs*, **71** (2024), 3810–3814. https://doi.org/10.1109/TCSII.2024.3370865
12. X. Wang, E. van Kampen, Q. Chu, P. Lu, Stability analysis for incremental nonlinear dynamic inversion control, *J. Guid. Control Dyn.*, **42** (2019), 1116–1129. https://doi.org/10.2514/1.G003791
13. P. Acquatella, E. van Kampen, Q. P. Chu, Incremental backstepping for robust nonlinear flight control, in *EuroGNC 2013, 2nd CEAS Specialist Conference on Guidance, Navigation & Control*, (2013), 1444–1463.
14. W. Li, X. Han, Y. Zhi, B. Wang, L. Liu, H. Fan, Adaptive finite-time incremental backstepping fault-tolerant control for flying-wing aircraft with state constraints, *Aerosp. Sci. Technol.*, **147** (2024), 108968. https://doi.org/10.1016/j.ast.2024.108968
15. Y. Wang, F. Yan, J. Chen, F. Ju, B. Chen, A new adaptive time-delay control scheme for cable-driven manipulators, *IEEE Trans. Ind. Inf.*, **15** (2019), 3469–3481. https://doi.org/10.1109/TII.2018.2876605
16. G. R. Cho, P. H. Chang, S. H. Park, M. Jin, Robust tracking under nonlinear friction using time-delay control with internal model, *IEEE Trans. Control Syst. Technol.*, **17** (2009), 1406–1414. https://doi.org/10.1109/TCST.2008.2007650
17. D. K. Han, P. Chang, Robust tracking of robot manipulator with nonlinear friction using time delay control with gradient estimator, *J. Mech. Sci. Technol.*, **24** (2010), 1743–1752. https://doi.org/10.1007/s12206-010-0516-z
18. H. Bae, M. Jin, J. Suh, J. Y. Lee, P. Chang, D. Ahn, Control of robot manipulators using time-delay estimation and fuzzy logic systems, *J. Electr. Eng. Technol.*, **12** (2017), 1271–1279. https://doi.org/10.5370/JEET.2017.12.3.1271
19. M. Jin, S. H. Kang, P. H. Chang, Robust compliant motion control of robot with nonlinear friction using time-delay estimation, *IEEE Trans. Ind. Electron.*, **55** (2008), 258–269. https://doi.org/10.1109/TIE.2007.906132
20. J. Ma, S. Yu, W. Hu, H. Wu, X. Li, Y. Zheng, et al., Finite-time robust flight control of logistic unmanned aerial vehicles using a time-delay estimation technique, *Drones*, **8** (2024), 58. https://doi.org/10.3390/drones8020058
21. D. K. Schmidt, J. Stevens, J. Roney, Near-space station-keeping performance of a large high-altitude notional airship, *J. Aircr.*, **44** (2007), 611–615. https://doi.org/10.2514/1.24863
22. Z. Zheng, Y. Zou, Adaptive integral LOS path following for an unmanned airship with uncertainties based on robust RBFNN backstepping, *ISA Trans.*, **65** (2016), 210–219. https://doi.org/10.1016/j.isatra.2016.09.008

23. T. Chen, M. Zhu, Z. Zheng, Asymmetric error-constrained path-following control of a stratospheric airship with disturbances and actuator saturation, *Mech. Syst. Signal Process.*, **119** (2019), 501–522. https://doi.org/10.1016/j.ymssp.2018.10.003

24. Y. C. Wang, W. S. Chen, S. X. Zhang, J. W. Zhu, L. J. Cao, Command-filtered incremental backstepping controller for small unmanned aerial vehicles, *J. Guid. Control Dyn.*, **41** (2018), 954–967. https://doi.org/10.2514/1.G003001

25. J. Pomet, L. Praly, Adaptive nonlinear regulation: Estimation from the lyapunov equation, *IEEE Trans. Autom. Control*, **37** (1992), 729–740. https://doi.org/10.1109/9.256328

26. M. Jin, J. Lee, P. H. Chang, C. Choi, Practical nonsingular terminal sliding-mode control of robot manipulators for high-accuracy tracking control, *IEEE Trans. Ind. Electron.*, **56** (2009), 3593–3601. https://doi.org/10.1109/TIE.2009.2024097

27. Y. Wang, Z. Zhang, C. Li, M. Buss, Adaptive incremental sliding mode control for a robot manipulator, *Mechatronics*, **82** (2022), 102717. https://doi.org/10.1016/j.mechatronics.2021.102717

AIMS Press